



OPEN ACCESS

EDITED BY

Zhiyuan Hu,
School of atmospheric sciences, Sun
Yat-sen University, China

REVIEWED BY

Zhicong Yin,
Nanjing University of Information
Science and Technology, China
Yongjing Ma,
Institute of Atmospheric Physics (CAS),
China
Bing Pu,
University of Kansas, United States

*CORRESPONDENCE

Xiaoyan Wang,
wangxyfd@fudan.edu.cn

SPECIALTY SECTION

This article was submitted to
Atmosphere and Climate,
a section of the journal
Frontiers in Environmental Science

RECEIVED 10 August 2022

ACCEPTED 30 September 2022

PUBLISHED 13 October 2022

CITATION

Sun Y and Wang X (2022),
Meteorological factor contributions to
the seesaw concentration pattern
between PM_{2.5} and O₃ in Shanghai.
Front. Environ. Sci. 10:1015723.
doi: 10.3389/fenvs.2022.1015723

COPYRIGHT

© 2022 Sun and Wang. This is an open-
access article distributed under the
terms of the [Creative Commons
Attribution License \(CC BY\)](https://creativecommons.org/licenses/by/4.0/). The use,
distribution or reproduction in other
forums is permitted, provided the
original author(s) and the copyright
owner(s) are credited and that the
original publication in this journal is
cited, in accordance with accepted
academic practice. No use, distribution
or reproduction is permitted which does
not comply with these terms.

Meteorological factor contributions to the seesaw concentration pattern between PM_{2.5} and O₃ in Shanghai

Yongzhao Sun¹ and Xiaoyan Wang^{1,2,3*}

¹Department of Atmospheric and Oceanic Sciences and Institute of Atmospheric Sciences, Fudan University, Shanghai, China, ²CMA-FDU Joint Laboratory of Marine Meteorology, Shanghai, China, ³Shanghai Institute of Pollution Control and Ecological Security, Shanghai, China

With the implementation of various stringent emission reduction measures since 2013 in China, significant declines in fine particle (PM_{2.5}) concentrations have occurred nationwide. However, China has suffered from increasing levels of ozone pollution in eastern urban areas. Many studies focus on the chemical interaction between PM_{2.5} and O₃, but the meteorological mechanisms of the seesaw variation pattern between them are still unclear. Taking the megacity Shanghai (SH) as an example, we explored the meteorological causes of two types of PM_{2.5}-O₃ concentration variation seesaw events, i.e., high PM_{2.5} concentration with low O₃ concentration (Type-one) events and low-PM-high-O₃ (Type-two) seesaw events. The backward trajectories of the 144 Type-one events are divided into three clusters. Among the three clusters of Type-one seesaw events, the boundary layer height decreases by 20.53%–53.58%, and the wind speed decreases by 17.99%–28.29%, which is unfavorable for the diffusion of local air pollutants and contributes to the accumulation of PM_{2.5}. Additionally, a backward air mass with a high content of PM_{2.5} plays an important role in the Type-one events, especially in the case of cluster one. In terms of cluster two, the increase in cloud cover, decrease in solar radiation and increase in relative humidity also promote the hygroscopic growth of aerosols and suppress the production of O₃. As for cluster three, higher cloud cover and relative humidity contribute to the seesaw pattern of PM and O₃. The 64 Type-two seesaw events are divided into two clusters. O₃-rich air masses from the nearby east sea surface and remote northeast China increase the local O₃ of SH. Moreover, in cluster one, high boundary layer depth and wet deposition contribute to the decrease in PM_{2.5} concentration. In cluster two, a obvious decrease in cloud cover and increase in solar radiation are also favorable for the photochemical production of ozone. The results will provide suggestions for the government to use to take measures to improve the air quality of SHs.

KEYWORDS

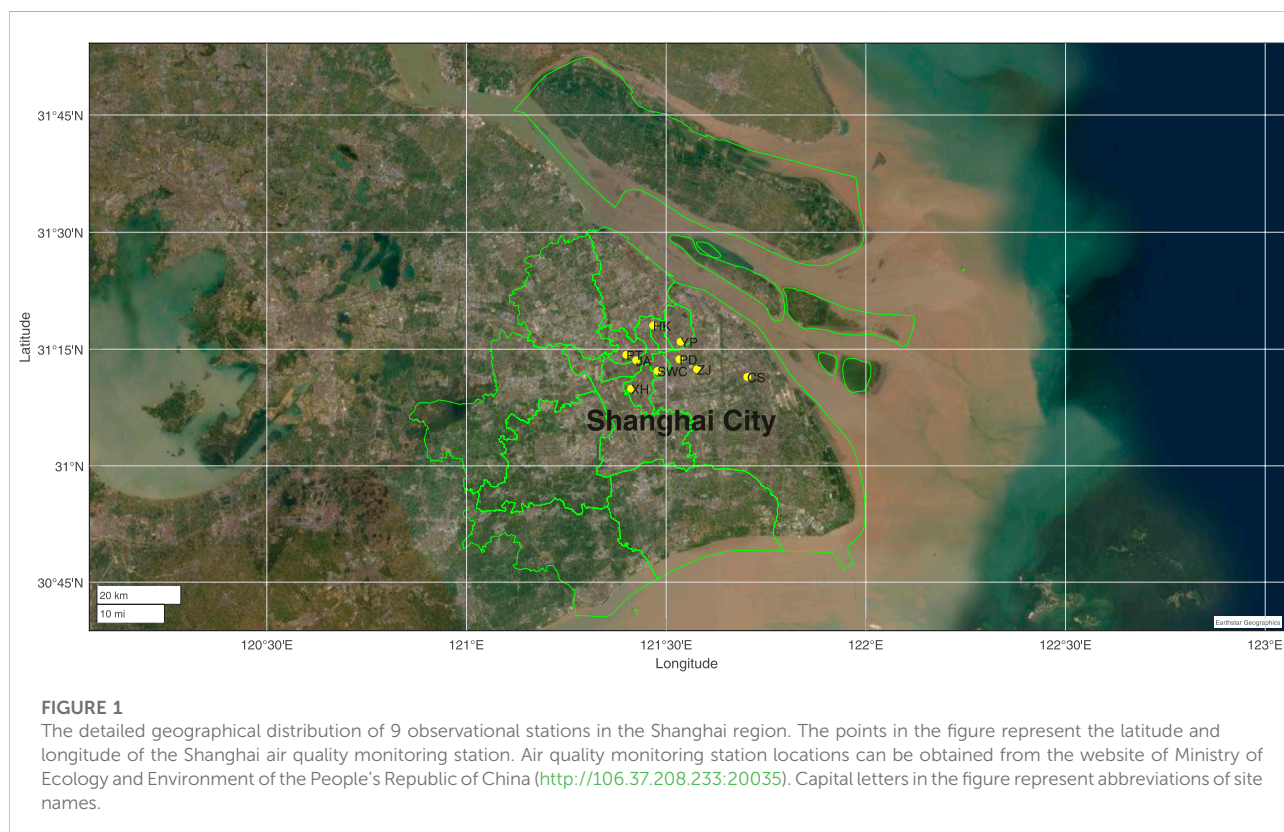
PM_{2.5}, O₃, meteorological mechanisms, Shanghai, backward trajectory

Introduction

In recent years, cities in eastern China have been facing severe air pollution. $PM_{2.5}$ (particles with aerodynamic diameters less than $2.5\ \mu m$) and ozone concentrations often exceed air quality standards (Ministry of Ecology and Environment, 2013). Air pollution is one of the main environmental problems in urban areas, particularly in megacities, such as Shanghai (SH). Exposure to high levels of $PM_{2.5}$ has adverse effects on human health and ecosystem productivity (Yue et al., 2017; Wang et al., 2019a). Thus, in September 2013, the State Council issued the Action Plan on the Prevention and Control of Air Pollution, known as the Clean Air Actions (CAA), to aggressively control anthropogenic emissions. The Yangtze River Delta region was required to reduce its $PM_{2.5}$ concentrations by 20% within 5 years (Ministry of Ecology and Environment, 2013). Starting that year, $PM_{2.5}$ data from a nationwide monitoring network of approximately 1000 sites became available from the China National Environmental Monitoring Center (CNEMC) of the Ministry of Ecology and Environment of China (MEE). Afterward, in a three-year action plan to fight air pollution (State Council of the People's Republic of China, 2018), sulfur dioxide, nitrogen oxides and $PM_{2.5}$ were further restricted. With joint efforts, the average annual $PM_{2.5}$ concentration in China decreased by 44% in 2019 compared with 2013 (Zhong et al., 2021). However, at the same time, the surface ozone concentration in China continues to rise (Liu et al., 2018; Dang and Liao, 2019, 2012–2017), which partially offsets the health benefits brought by the decrease in $PM_{2.5}$ concentration.

Stage II of the CAA plan began in 2018 (State Council of the People's Republic of China, 2018), and new emission control measures were implemented for surface ozone.

Given the seesaw variation between $PM_{2.5}$ and O_3 , i.e., the decrease in O_3 concentrations with the increase in $PM_{2.5}$ contents, many studies have been conducted to investigate the chemical mechanisms (Shao et al., 2022; Wu et al., 2022). The interaction between $PM_{2.5}$ and O_3 is closely related and very complicated. NO_x and VOCs (volatile organic compounds) in the atmosphere are able to generate ozone under light conditions in photochemical reactions (Carrillo-Torres et al., 2017). In this process, NO_x , SO_2 and VOCs are also oxidized to form secondary $PM_{2.5}$ (Zhu et al., 2015). At nighttime and in the immediate vicinity of large NO emissions, ozone concentrations are depressed through the process of NO_x titration. The result is the net conversion of O_3 to NO_2 (Gillani and Pleim, 1996). In regions with high NO_x emissions, O_3 formation can be VOC-limited (Sillman et al., 1990; Kleinman et al., 2003). As a result of CAA, NO_x decreased obviously (Silver et al., 2018, 2015–2017). Thus, due to the nonlinear relationship between O_3 production and NO_x (Simon et al., 2015), the concentration of O_3 in VOC-limited areas in eastern China increases to some extent. Through heterogeneous chemical reactions, $PM_{2.5}$ can indirectly affect O_3 . In winter on the North China Plain, formaldehyde is produced by the oxidation of reactive VOCs. The fast production of ozone is driven by HOx radicals from the photolysis of formaldehyde, overcoming radical titration from the decreased NO_x emissions (Li et al., 2021). Research has demonstrated an ~40% decrease in $PM_{2.5}$, slowing the aerosol sink of hydroperoxyl (HO₂) radicals



and thus stimulating ozone production at 0.6–1 ppbv a⁻¹ in Beijing–Tianjin–Hebei (Li et al., 2019). Using the WRF-CMAQ model, Liu and Wang also uncovered a similar and substantial effect of HO₂ uptake on increases in O₃ levels due to changes in PM concentrations (Liu and Wang, 2020a). Although many studies have been performed to evaluate the quantitative contributions of photolysis rates and heterogeneous chemical reactions to the production of O₃, their relative importance is still unclear (He and Carmichael, 1999; Sillman, 1999).

The absorption and scattering of shortwave radiation by PM_{2.5} can attenuate incident solar shortwave radiation and change the radiation balance in the atmosphere (Charlson et al., 1992; Bond et al., 2013). The attenuation of short-wave radiation will reduce the photolysis rate of O₃ and precursors (J [O₃¹D] and J [NO₂], etc.), which will decrease the photochemical reaction intensity, and then reduce the net chemical production of O₃ (Jacobson, 1998; Li et al., 2011; Deng et al., 2012). Wang et al. (2019b) analyzed the photolysis rate data in Beijing from 2012 to 2015, and found that aerosols caused J[NO₂] and J[O₃¹D] near the ground in Beijing to decrease by 24%–30% and 27%–33%, respectively, which led to a decrease of photochemical generation rate in the local ozone in summer by approximately 25%.

Previous studies on the interaction between PM_{2.5} and O₃ have mostly focused on chemical mechanisms. However, meteorological conditions also have great effects on the formation, transportation and deposition processes of PM_{2.5} and O₃ and their precursors (Finlayson-Pitts and Pitts, 1986; Cox and Chu, 1996; Xu et al., 1996; Mu and Zhang, 2014; Zhang et al., 2014; Hu et al., 2015; Yin et al., 2017; Zhang, 2017; Wang et al., 2021). For example, by altering the chemical reaction rates directly and the biogenic emissions of VOCs indirectly, higher temperatures can enhance ozone formation in most instances (Guenther et al., 2006; Lu et al., 2019b). The response of PM_{2.5} concentrations to temperature was largely the result of

competing changes in sulfate and nitrate concentrations with a smaller role played by organics (Dawson et al., 2007). Increasing relative humidity will increase the water content of fine particles, thus increasing the PM_{2.5} concentration (Dawson et al., 2007). Water vapor is able to react with the excited oxygen atom O(¹D) and generate OH radicals, which eventually lead to a reduction in the reaction between O(¹D) and O₂ (Johnson et al., 1999). Thus, the increase in water vapor can lead to a decrease in surface ozone concentrations (Camalier et al., 2007; He et al., 2017). Pollutant distributions are strongly affected by the wind field (Chen et al., 2020). PM_{2.5} concentrations typically decrease by an order of magnitude between polluted regions and the diluting background air, whereas for ozone concentrations may actually increase or decrease, affected by upwind regions (Jacob and Winner, 2009; Gu et al., 2020b). Precipitation decreases both PM_{2.5} and O₃ concentrations *via* wet removal (Shan et al., 2008). An increase in the planetary boundary layer height can decrease pollutant levels *via* dilution of primary pollutants into a larger volume of air (Su et al., 2018)

However, most of the existing studies focused on the meteorological condition contributions to the individual pollution of PM_{2.5} or O₃ (He et al., 2017; Wang et al., 2018; Lu et al., 2019a; Zhai et al., 2019; Li et al., 2020; Yin et al., 2020). In terms of the synergetic seesaw pattern between PM_{2.5} and O₃, its meteorological mechanism has been poorly understood. Individual meteorological factors will have the same or adverse effects on the concentration of PM_{2.5} and O₃. What is the net contribution of meteorological conditions to the seesaw concentrations pattern between PM_{2.5} and O₃. This study will take the seesaw concentration events of PM_{2.5} and O₃ in Shanghai as a case to reveal their meteorological causes, which will benefit the prediction of future synergetic pollution of PM_{2.5} and O₃.

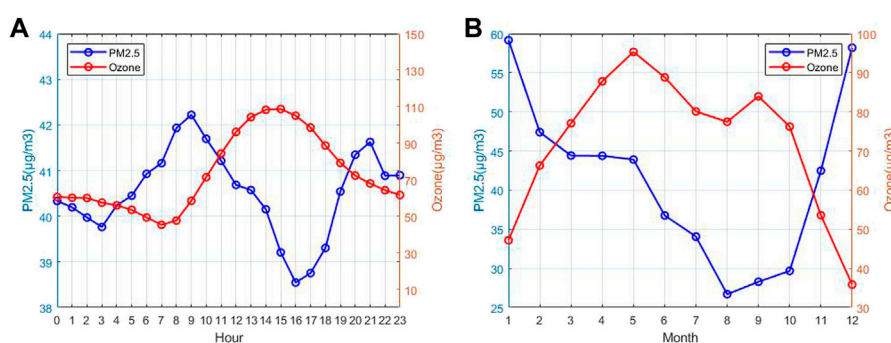


FIGURE 2

The hourly and seasonal means of PM_{2.5} and ozone concentrations in Shanghai, (A) diurnal changes and (B) monthly changes from 2014 to 2020.

Data and method

Air pollution dataset

Hourly surface observations of O₃, PM_{2.5} and nitrogen dioxide (NO₂) were all obtained from the CNEMC network (<http://106.37.208.233:20035/>, last access: 28 December 2020). As part of the CAA, the network started in 2013 with 496 sites in 74 major cities across the country, growing to more than 2500 sites in 366 cities by 2020. At each monitoring site, the concentration of O₃ was measured using ultraviolet absorption spectrometry and differential optical absorption spectroscopy. PM_{2.5} mass concentrations are measured using the micro-oscillating balance

method and/or the β absorption method. NO₂ concentrations are measured by the molybdenum converter method, which is known to have positive interferences from NO₂ oxidation products (Ministry of Ecology and Environment, 2012). Instrumental operation, maintenance, data assurance, and quality control were conducted based on the most recent revisions of China’s environmental protection standards (Ministry of Ecology and Environment, 2013). In terms of time, all the data we used are from 13 May 2014 to 7 November 2020.

Air quality data were measured at 9 sites in the Shanghai region, and each site has distinct representation for different influences from urban air pollutant emissions. Figure 1 shows the locations of the nine sites, i.e., Putuo Station, No.15 Factory

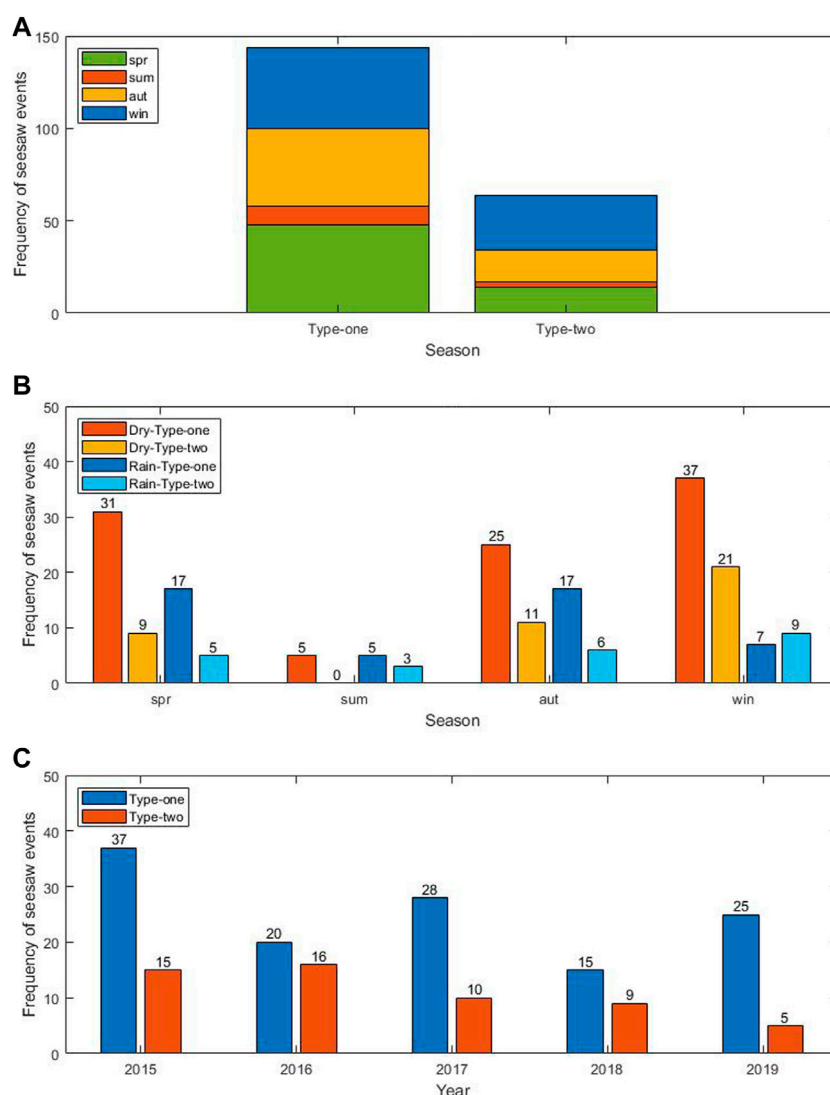


FIGURE 3 The seasonal distribution (A), precipitation distribution (B) and annual distribution (C) of seesaw events in Shanghai during 2013–2020. If the hourly precipitation of any grid exceeds 0.5 mm, it is considered that there is an obvious wet cleaning process in this study.

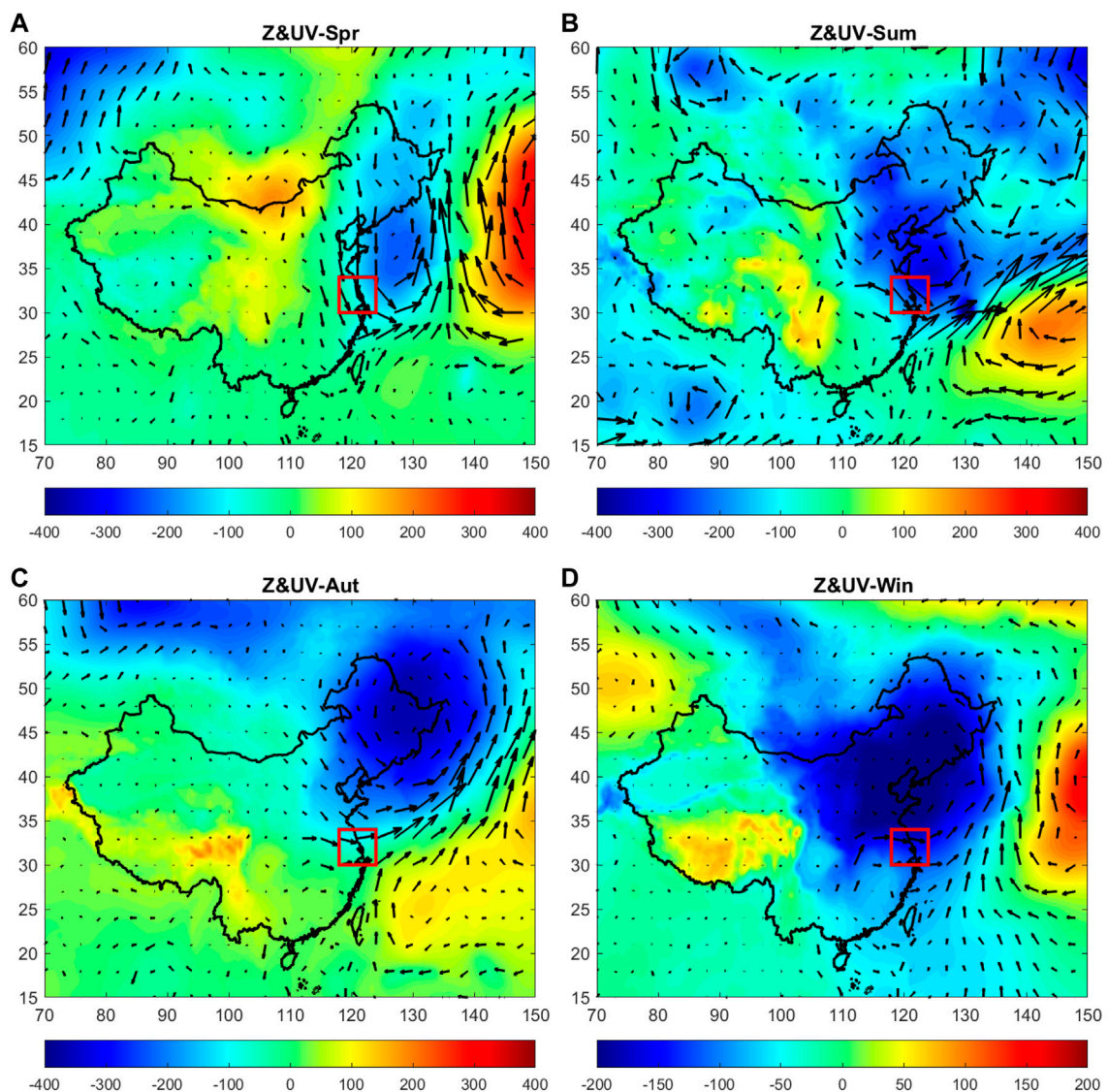


FIGURE 4

Seasonal anomaly of atmospheric circulation at 925 hPa for the Type-one seesaw events. The shading indicates the anomaly of geopotential height (unit: $\text{m}^2\cdot\text{s}^{-2}$). The black arrow is the wind anomaly. The solid red box marks the location of Shanghai. And the results are shown for (A) spring, (B) summer, (C) autumn, (D) winter.

Station, Hongkou Station, Xuhui Shanghai Normal University Station, Yangpu Sipiao Station, Jing'an Monitoring Station, Pudong Chuansha Station, Pudong New Area Monitoring Station and Pudong Zhangjiang Station. As the observation system is being developed and gradually improved, the duration of available data varies from station to station. The concentration unit of air quality data provided by the official website of MEE is micrograms per cubic meter ($\mu\text{g}\cdot\text{m}^{-3}$). Before 31 August 2018, the concentration was under the standard condition (273 K, 1013 hPa). From 1 September 2018 and on, the reference gas concentration was changed to 298 K and

1013 hPa, and the $\text{PM}_{2.5}$ concentration was changed to the measured local environmental conditions. Additionally, we removed invalid values and abnormal values from the hourly CNEMC data due to instrument calibration issues.

Meteorological dataset

The hourly dataset of the fifth-generation European Centre for Medium-Range Weather Forecasts (ECMWF ERA5) atmospheric reanalysis dataset with a resolution of 0.25° was

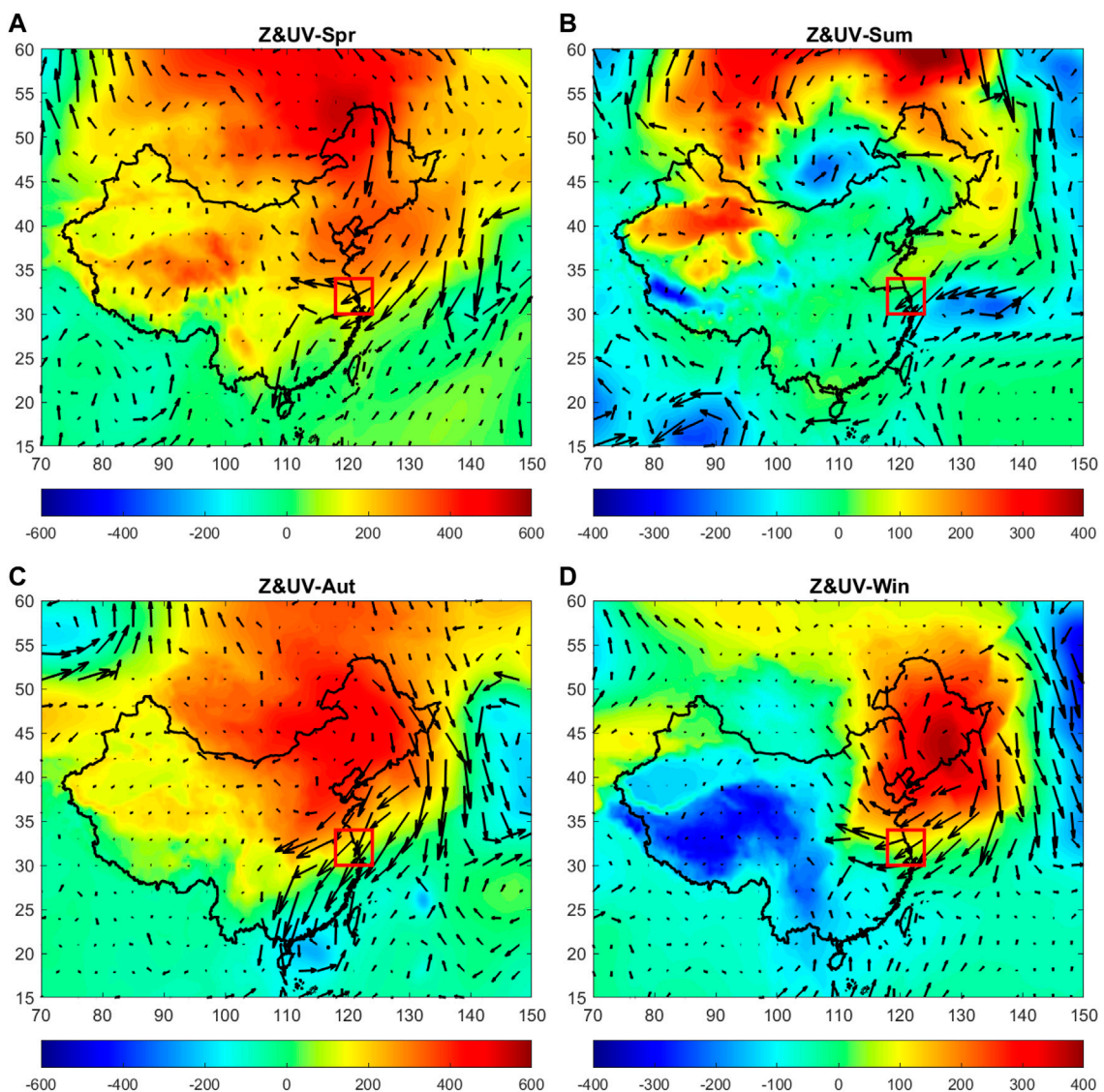


FIGURE 5

The same as in Figure 4 but for the Type-two events. The solid red box marks the location of Shanghai. And the results are shown for (A) spring, (B) summer, (C) autumn, (D) winter.

used to describe the meteorological characteristics in this research (<https://cds.climate.copernicus.eu/cdsapp#!/dataset/reanalysis-era5-pressure-levels?tab=overview>, <https://cds.climate.copernicus.eu/cdsapp#!/dataset/reanalysis-era5-single-levels?tab=overview>, last access: 18 May 2022). The U and V components of 10 m wind, 2 m air temperature, relative humidity, boundary layer height (BLH), mean surface downward longwave radiation flux (Longwave), mean surface downward shortwave radiation flux (Shortwave), total precipitation, fraction of cloud cover, surface net solar radiation (SSR), and the vertical distribution of vertical velocity, geopotential, and ozone mass mixing ratio are

involved in this study. In order to find out the statistical difference between meteorological variable values of five clusters, *t*-test is used to examine significance. The *t*-test is a popular statistical tool used to test differences between the means of two groups, or the difference between one group's mean and a standard value. Running *t*-tests help us to understand whether the differences are statistically significant (Box, 1987).

Additional information on ozone in ERA5 is that the heterogeneous ozone chemistry is updated and the interaction between ozone and the atmosphere is one-way. Ozone is advected by the atmospheric flow. However, the

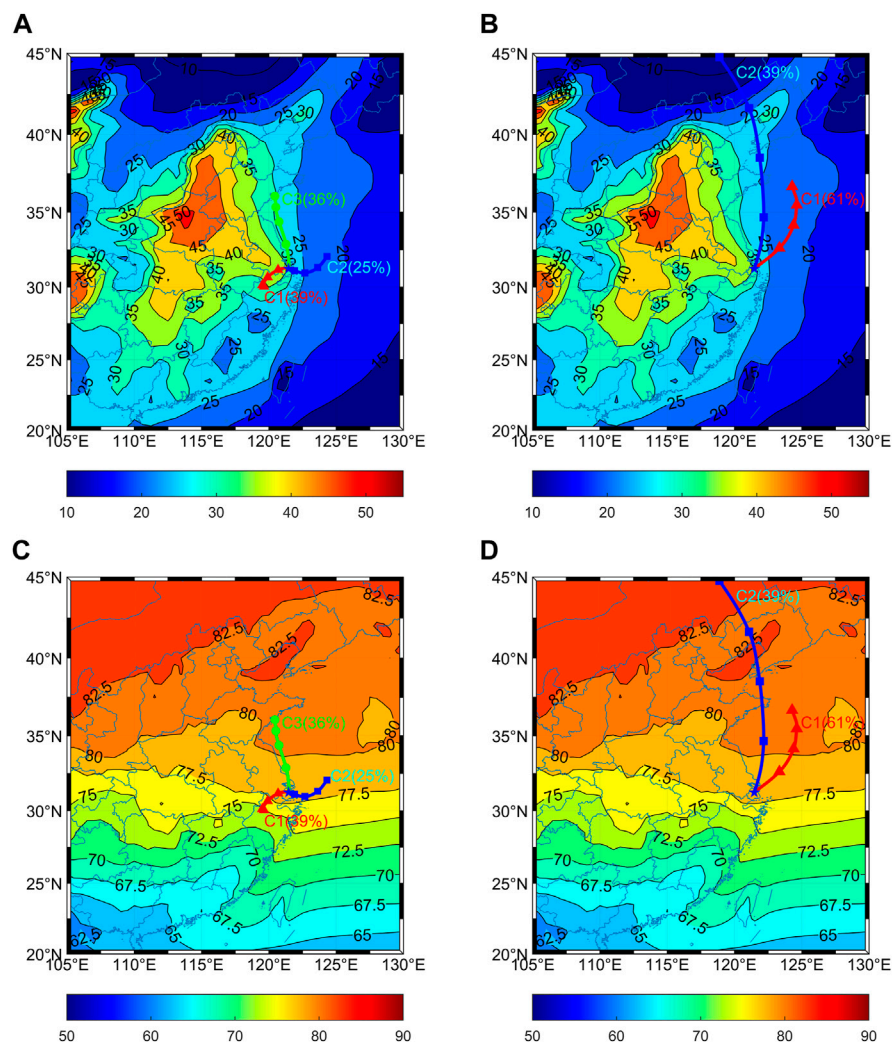


FIGURE 6

Transport pathways of air masses in 5 clusters with (A,B) PM_{2.5} mean concentration and (C,D) O₃ mean concentration (ppb). The background PM_{2.5} concentration is the annual average from 2014 to 2020, sourced from MERRA-2. The background ozone concentration is the annual average from 2014 to 2020, sourced from ERA5.

ERA5 prognostic ozone has no feedback on the atmosphere *via* the radiation scheme (Hersbach et al., 2020).

Since it has a relatively high temporal and spatial resolution (1 hour averages and $0.5^\circ \times 0.625^\circ$), we also obtain surface PM_{2.5} concentrations in the Modern-Era Retrospective Analysis for Research and Applications, version 2 (MERRA-2). Using fields from the 2D aer_Nx collection, the concentration of particulate matter can be computed using the following formula:

$$PM_{2.5} = DUSMASS25 + OCSMASS + BCSMASS + SSSMASS25 + SO4SMASS * (132.14/96.06)$$

Because the species tracer in MERRA-2 is the sulfate ion, sulfate requires a multiplication factor (<https://gmao.gsfc.nasa.gov/reanalysis/MERRA-2/FAQ/>). In addition to the lack of nitrate aerosols

in MERRA-2, the bias in MERRA-2 mainly comes from the uncertainties of the emission inventory and meteorological simulation in GOES-5 (Geostationary Operational Environmental Satellite-5) models (Buchard et al., 2016; He et al., 2019).

Definition of seesaw events of PM_{2.5} and O₃

As shown in Figure 2, the PM_{2.5} concentration and O₃ concentration in SH have obvious seasonal and diurnal seesaw variation characteristics. Figure 2 shows the climatology of

TABLE 1 Absolute anomalies and relative anomalies of PM_{2.5}, O₃ and NO₂ concentrations in each backward trajectory cluster of the two seesaw events in Shanghai. Units: μg/m³. The anomalies are with respect to their average value of every hour in every month.

Pollutants	Cluster1	Cluster2	Cluster3
Type-one			
PM _{2.5}	+49.84	+40.45	+45.22
O ₃	-33.19	-39.49	-33.63
NO ₂	+41.06	+30.61	+22.77
Type-two			
PM _{2.5}	-33.88	-40.34	
O ₃	+25.77	+22.65	
NO ₂	-22.83	-33.87	

TABLE 2 Relative anomaly percent changes in PM_{2.5}, O₃ and NO₂ concentrations in each backward trajectory cluster of the two seesaw events in Shanghai. Units: %. The relative anomalies are with respect to the average value of every hour in every month.

Pollutants	Cluster1	Cluster2	Cluster3
Type-one			
PM _{2.5}	+107.54%	+95.92%	+105.65%
O ₃	-58.45%	-54.70%	-54.56%
NO ₂	+82.88%	+71.88%	+51.81%
Type-two			
PM _{2.5}	-67.97%	-71.09%	
O ₃	+53.18%	+64.25%	
NO ₂	-46.61%	-57.64%	

diurnal and seasonal variations in PM_{2.5} and O₃ concentrations. It shows higher PM_{2.5} concentrations during the morning rush hour and lower concentrations in the afternoon; while O₃ shows lower concentrations at 7–8 a.m. and higher concentrations at 2–3 p.m. In terms of seasonal variation, the PM_{2.5} concentration in winter is the highest, but winter is the cleanest season for O₃ pollution in SH. The chemical and physical mechanisms of the diurnal and seasonal seesaw pattern between PM_{2.5} and O₃ in Figure 2 have been revealed in previous studies from the perspective of the variation in emission and meteorological factors. In short, ozone has a strong correlation with high temperatures, so it peaks at midday and during mid-spring to early summer in SH (Gu et al., 2020a; Chang et al., 2021). The reason that ozone concentration of Shanghai in spring is higher than summer is the photochemical reaction of ozone affected by plum-rain in summer (Gao et al., 2017). Deep and persistent cloud cover impedes solar radiation to reach the surface of the Earth, affecting the photochemical generation of ozone Affected by human activities, household heating in winter and vehicle emissions in the morning and evening are able to increase PM_{2.5} (Xiao et al., 2015; Zhang and Cao, 2015). Outbreaks of haze

generally occur during the winter as a result of temperature inversions. During an inversion warm air settles above a layer of cool air near the surface. The lid-like warm air traps pollutants near the surface. Lower PM in afternoon can be explained by the enhanced emission for heating and relatively low the boundary layer (Zhang and Cao, 2015). However, there are still some seesaw events of PM_{2.5} and O₃ under the background of diurnal and seesaw patterns shown in Figure 2, the mechanisms of which are still unclear. This study will focus on the meteorological causes of these seesaw events.

To eliminate the influence of seasonal variation, diurnal variation and interannual variation, the original data are classified according to different years, months and hours, and the mean, first quartile and third quartile are calculated. The original data of PM_{2.5} and O₃ are compared with the corresponding quartile. If the hourly concentration of PM_{2.5} is greater than the corresponding third quartile, and O₃ is less than the corresponding first quartile, we call it High-PM-Low-O₃ seesaw hour (Type-one for short). Similarly, if the hourly concentration of O₃ is greater than the corresponding third quartile, and PM_{2.5} is less than the corresponding first quartile, it is defined as Low-PM-High-O₃ hour (Type-two). The quartiles are not fixed, but change with the specific year, month and hour. The above three influencing factors, together with the original data of pollutant concentration, any change in four variables will affect the quartiles. That is, the relatively high/low air pollutant concentrations are used to define the seesaw cases instead of their absolute values. To ensure the spatial and temporal continuity of the two types of cases, a seesaw event was defined as at least 12 consecutive seesaw hours occurring at more than half of the available observation stations in Shanghai.

HYSPLIT model and clustering analysis

Backward trajectory analysis essentially follows a parcel of air backward in hourly time steps for a specified length of time. The Hybrid-Single Particle Lagrangian Integrated Trajectory (HYSPLIT) model (Draxler et al., 2009) developed by the National Oceanic and Atmospheric Administration (NOAA) was used in this study to identify potential source regions of PM_{2.5} or O₃ for a specific city of SH and capture the horizontal movement of the air masses from the source region. The model uses internal terrain following sigma coordinates and meteorological element fields are interpolated linearly to the corresponding coordinates.

To show the origins of air masses arriving at SH, 48-hour backward trajectories were computed every 6 h (at 00:00, 06:00, 12:00, and 18:00 UT) for the years 2014–2020 for 100 m above ground over SH using the HYSPLIT-4 model (Draxler et al., 2009). Meteorological archive data used for the HYSPLIT model are from NCEP (National Centers for Environmental Prediction), at a horizontal resolution of 2.5° (latitude) × 2.5° (longitude).

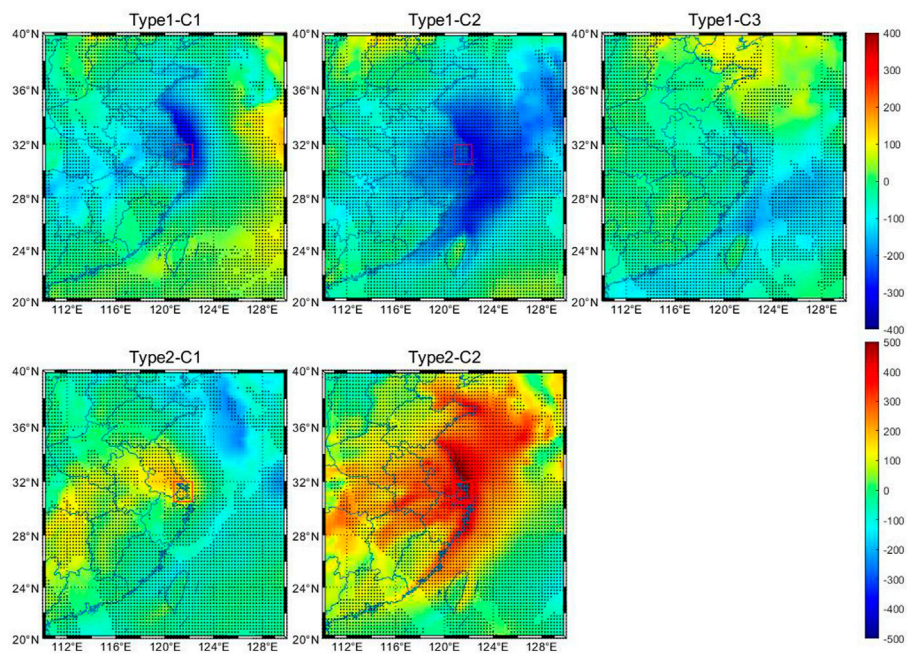


FIGURE 7

Anomalies of boundary layer height in 5 clusters. The solid blue line in the background indicates the provincial boundaries of China. Different subtitles represent different clusters. The black dots indicate that the grids are above the 99% confidence level ($p < 0.01$). The solid red box marks the location of Shanghai. Unit: m.

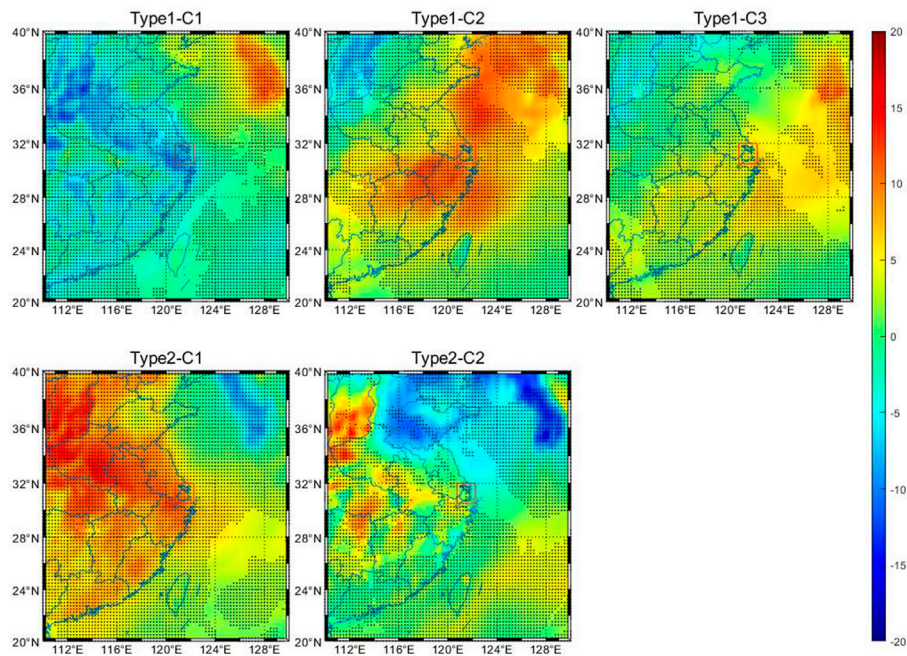


FIGURE 8

Anomalies of relative humidity in 5 clusters. The solid blue line in the background indicates the provincial boundaries of China. Different subtitles represent different clusters. The black dots indicate that the grids are above the 99% confidence level ($p < 0.01$). The solid red box marks the location of Shanghai. Unit: %.

TABLE 3 Meteorological factor percent changes in 5 clusters. The bold font indicates an important influencing factor. Units: % Data source: ERA5-1000 hPa & Surface. The relative anomalies are with respect to the average value of every hour in every month. Bold fonts indicate the main factors influencing the specific seesaw cluster.

Variable	Cluster1	Cluster2	Cluster3
Type-one			
Temperature	-3.27%	+11.18%	-0.27%
BLH	-53.58%	-48.13%	-20.53%
Shortwave	+2.91%	-20.96%	-9.67%
Longwave	-3.15%	+6.75%	+0.95%
SSR	+1.78%	-15.70%	-6.48%
Precipitation	-32.76%	+32.25%	-33.55%
Windspeed	-28.29%	-39.11%	-17.99%
Cloud Cover	+2.62%	+24.92%	+8.69%
Relative Humidity	-9.89%	+12.78%	+5.80%
Type-two			
Temperature	+21.75%	-22.80%	
BLH	+45.63%	+100.02%	
Shortwave	-18.87%	+6.27%	
Longwave	+7.08%	+0.84%	
SSR	-13.94%	+3.90%	
Precipitation	+136.85%	-40.58%	
Windspeed	+38.35%	+38.88%	
Cloud Cover	+37.10%	-51.40%	
Relative Humidity	+13.22%	+1.60%	

TrajStat software is used to classify the backward trajectories arriving at SH to better determine the transportation of PM_{2.5} and O₃. The trajectories were assigned to distinct clusters according to their moving speed and direction using Ward's hierarchical method based on the Euclidean distance between all pairs of trajectories (Sirois and Bottenheim, 1995). Major transport pathways leading to elevated or dropped PM_{2.5} concentrations and ozone concentrations were identified by combining trajectories with the corresponding mean concentrations of the pollutant.

Results

Occurrence frequency of the seesaw events

Figure 3A shows the seasonal distribution of the two types of PM_{2.5} and O₃ seesaw events during the 2013–2020 period. Obviously, the frequency of Type-one seesaw events is higher than Type-two in total. There were 144 cases in Type-one and 64 cases in Type-two. In terms of seasons, most of the two types of seesaw events occur in winter. Both seesaw events show the lowest frequency in summer, which is approximately 22.73% and 10% of that in winter for Type-one and Type-two, respectively.

Considering the wet deposition, the physical mechanisms of the seesaw events are supposed to be different from those on dry days. We reclassified the seesaw events with the occurrence of precipitation in Figure 3B. In summer, more than half of the seesaw events occurred on rainy days, which is different from other seasons. The sample size is 5 for both dry and rainy Type-one events in summer, but all the Type-two events occur on rainy days. The positive correlation between PM_{2.5} and O₃ in summer results in the lowest event frequency occurring in summer. High O₃ concentrations in a strong oxidative air condition promoted the formation of secondary particles in summer. During plum-rain in summer, under most circumstances PM_{2.5} concentrations and O₃ concentrations decrease at the same time due to precipitation (Jia et al., 2017; Zhu et al., 2019). The interannual variation in the seesaw event frequency is shown in Figure 3C.

Atmospheric circulation anomalies of the seesaw events

The roles of meteorology on pollutants are complex and varying. To further explore the meteorological causes behind the seesaw incidents, we calculated the anomalies of meteorological variables under the seesaw events in different seasons, including geopotential height (Z) and U/V components at 925 hPa, 850 hPa and 500 hPa. Figure 4 indicates the seasonal average of Z&UV anomalies at 925 hPa for Type-one seesaw events (i.e., high PM_{2.5} with low O₃ concentrations). It shows almost the same atmospheric circulation pattern in the four seasons, with a cyclonic anomaly over North China and the Northeast China region, which brings northwest or west winds to SH. For the case of Type-two seesaw events in Figure 5 (i.e., high O₃ with low PM_{2.5} concentrations), the circulation anomalies are also the same in spring, autumn and winter. SH is located at the edge of the west positive and east negative pressure, and the prevailing wind of SH comes from the northeast. In terms of the summertime, the sample size of Type-two is small, which leads to the vague distribution of its circulation anomaly pattern. The atmospheric circulation anomalies at 850 hPa and 500 hPa also show the same pattern for each type of seesaw event (figures not shown here). According to Figures 4, 5, there is almost no difference in the seasonal circulation anomalies, therefore, we investigate the mechanisms of seesaw events without considering their seasonal difference hereafter.

Regional transport contributes to the seesaw events

Although it shows a consistent seasonal circulation anomaly distribution for each type of seesaw events in Figures 4, 5, it

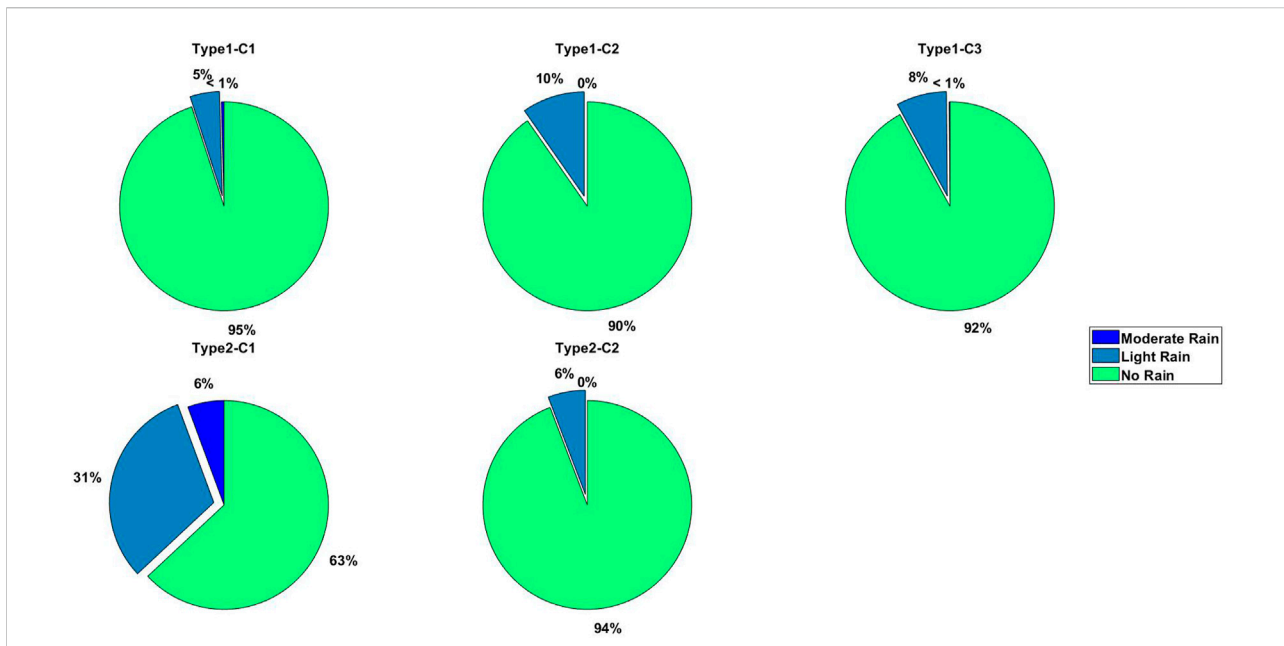


FIGURE 9 Precipitation intensities in 5 clusters of Shanghai seesaw events. No rain: the rate of fall varying between a trace and 0.5 mm per hour. Light rain: the rate of fall varying between 0.5 mm and 2.5 mm per hour. Mild rain: the rate of fall varying between 2.5 mm and 7.6 mm per hour (American Meteorological Society).

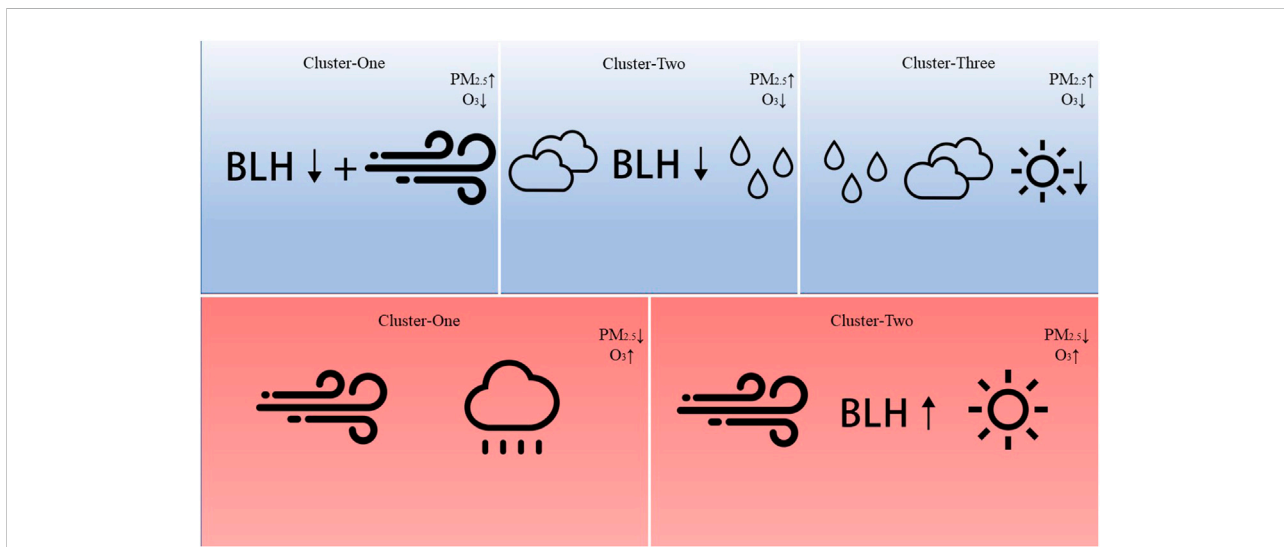
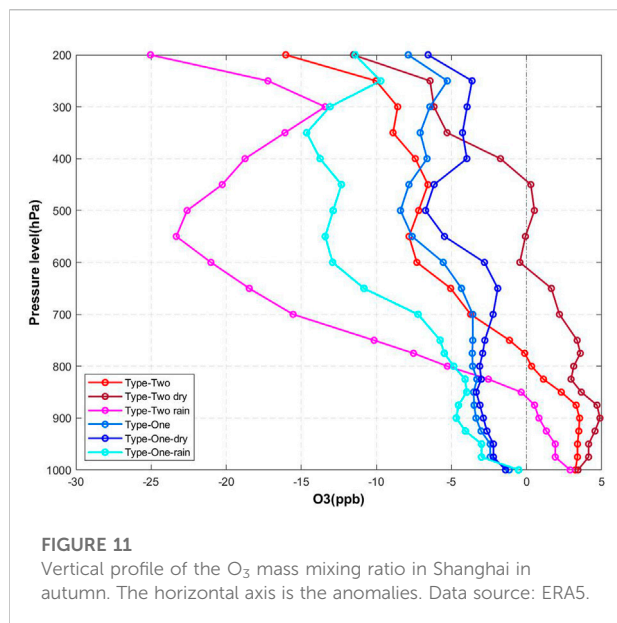


FIGURE 10 Diagram of the impacts of meteorology on both the O_3 and $PM_{2.5}$ concentrations in Shanghai during seesaw events.

indicates an average pattern of atmospheric circulation. To reveal the mechanism of the specific seesaw event, the 48 h backward trajectory of each seesaw events is calculated and clustered, which can provide the information on the origins and transport

pathways of air masses. As shown in Figure 6, cluster analysis yielded a total of three air-mass clusters for the 144 Type-one seesaw events, and two air-mass clusters for the 64 Type-two events.



For the case of Type-one events, the three kinds of air masses in SH come from the eastern ocean, north China and southwest of SH. The frequencies of these three kinds of air masses are almost the same. There are 56 samples in C1, 36 samples in C2 and 52 samples in C3. Tables 1, 2 summarize the anomalies of PM_{2.5}, O₃ and NO₂ concentrations in each backward trajectory cluster. For Type-one seesaw events, the magnitudes of PM_{2.5} anomalies are higher in cluster-one (C1 for short) (+107%) and cluster-three (C3) (+105%) than cluster-two (+95%), which may be due to the higher PM_{2.5} background concentrations transported from the north and southwest upwind regions of SH (as shown in Figure 6). Moreover, the NO₂ concentration increased by 83% and 52% in C1 and C3 in the Type-one events, respectively, which can also imply the regional transportation of aerosols and precursors.

In terms of Type-two seesaw events, the air mass in SH mainly comes from the nearby east sea surface (61% of events, 39 samples) with minor influence from the remote northeast China (39% of events, 25 samples) Compared to the average pollutant concentrations, the PM_{2.5} concentrations of the two types of clusters decreased by 67.97% and 71.07%, respectively. Correspondingly, the ozone concentration increased by 53.18% and 64.25%, respectively. Based on the climatology of O₃ and PM_{2.5} in Figure 6, it shows higher O₃ concentrations and lower PM_{2.5} contents in the east sea surface. The easterly wind brings O₃-rich and low PM_{2.5} air masses to SH, and leads to high O₃ and low PM_{2.5} pollution for the two clusters of Type-two events. Several studies have found that ozone tends to be continuously produced in the downwind regions of major cities (Kleinman et al., 2003; Tie et al., 2009, 2013). O₃ formation usually occurs under strong VOC-limited conditions in coastal megacities, which inhibits O₃ chemical production. In the downwind

region, O₃ formation shifts to NO_x-limited conditions gradually on the contrary to the sea surface, which results in pronounced O₃ production (Kley, 1997). O₃ precursors emitted from a coastal city are advected to the ocean by land breezes and produce O₃ over the ocean, the O₃-rich air mass can be advected back to the city by sea breezes.

Meteorological cause for the seesaw events

The meteorological influence on the pollutant varied by region and could be comparable to or even more significant than the impact of changes in anthropogenic emissions (Liu and Wang, 2020b). The relative anomalies of air temperature, BLH, shortwave, longwave, SSR, precipitation, 10 m wind, cloud cover and relative humidity are involved to reveal the meteorological effects on seesaw events. Figures 7, 8 show the spatial distribution of BLH and RH relative anomalies in the five clusters. Table 3 summarizes the regional mean relative anomalies of the above nine meteorological factors of SH in the five clusters. For the case of C1 in Type-one events, it shows lower than normal BLH around SH and the East Ocean, with a significant negative BLH relative anomaly of 199.41 m (-54%). The BLH indicates the vertical diffusion ability of the local atmosphere, which has been demonstrated to have a negative relationship with ambient PM_{2.5} concentrations (Wang and Wang, 2014; Wang and Wang, 2016). The lower PM_{2.5} in C1 of Type-one events can be attributed to the repression of vertical diffusion to some extent. Considering that the wind speed drops by 0.93 m/s (-28%), stable and stagnant circulation may also increase the concentration of pollutants.

For C2 in Type-one, the height of the boundary layer decrease by 48.13% and the relative humidity increased by 12.78%, which is the most significant among the three clusters (Figure 8). Figure 9 shows the occurrence frequency of precipitation during the five clusters. Due to the positive precipitation anomaly (Table 3) and easterly backward trajectory (Figure 6), there is a positive relative humidity anomaly in C2 of Type-one events, which is beneficial for the hygroscopic growth of aerosols and leads to an increase in PM_{2.5} concentration (Wang et al., 2019b; Won et al., 2021). The scavenging process and physical removal mechanism of PM are determined by different precipitation intensities (Andronache, 2003; Chate et al., 2003; Wang et al., 2010). According to the definition of the American Meteorological Society, precipitation can be classified as light rain, mild rain and heavy rain (American Meteorological Society American Meteorological Society, 2022). Using this definition, Figure 9 shows the distribution of no rain, light rain and mild rain under the five clusters. The precipitation in C2 is primarily light rain, and the deposition ability is weak compared to moistening the air mass. The stable air mass also contributes to the accumulation of

surface air pollutants. In addition, based on the regional mean meteorological factor anomalies in Table 3, the significant increase in cloud cover (+25%) and decrease in shortwave radiation (−21%) on the rainy days also caused the weakening of ozone photochemical production, which led to the decrease in surface ozone concentration in Shanghai.

For C3 in Type-one, the magnitudes of the regional mean meteorological anomalies are not as obvious as those in C1 and C2. However, the obvious increase in relative humidity (+5.8%) and decrease in solar radiation (−9.7%) can be considered a beneficial meteorological background for the increase of PM_{2.5} and decrease of O₃, respectively. Notably, the C3 air mass comes from the North China Plain where the concentration of fine particles is generally high (Figure 6). This may indicate that the high concentration of PM_{2.5} in C3 is related to transport. In brief, it is the comprehensive influence of transport, shortwave radiation and relative humidity resulting in C3 (Figure 10).

As described in the previous section, regional transport is undoubtedly the main influencing factor of the Type-two seesaw events. The trajectory in Figure 6 also shows that the air masses originate from areas with higher ozone and lower PM concentrations. Apart from that, other meteorological factors also make sense. In C1 of Type-two, the simple size of the dry-day case is small, and only the rainy cases are involved. Apparently, it shows a obvious positive anomaly of precipitation (Table 3) and relative humidity (Figure 8). Compared with the case of C2 in Type-one, the frequency of moderate rain in C1 of Type-two is much higher. The effects of wet deposition are more pronounced than the hygroscopic growth of aerosols in a humid environment, which results in a decrease in PM_{2.5} (Jacob and Winner, 2009).

In C2 of Type-two events, a 51% decrease in cloud cover along with a 6.27% increase in shortwave radiation contributes to the photochemical formation of ozone. Moreover, the increase in solar radiation prompts the development of boundary layer, which results in the positive BLH anomaly by 403.28 m (+100%) and the improvement in atmospheric vertical diffusion conditions. The surface wind speed, which is regularly considered the metric of horizontal diffusion ability, increases by 39% in C2 of Type-two events. The significant improvement of vertical and horizontal diffusion conditions led to a decrease in the PM_{2.5} concentration (Wang et al., 2016; Wang et al., 2018; Wang and Zhang, 2020).

Conclusions and discussion

This study explored the impact of meteorological factors on the seesaw concentration pattern between PM_{2.5} and O₃ in Shanghai from 2014 to 2020. On the basis of the variation in PM_{2.5} and O₃ concentrations, we divided the seesaw events into two types, Type-one (High-PM-Low-O₃) and Type-two (Low-PM-High-O₃). The trajectories of the seesaw events were assigned to distinct clusters

according to their moving speed and direction using the HYSPLIT model. The specific number of clusters is given as follows: three clusters in Type-one and two clusters in Type-two.

In Type-one seesaw events, the boundary layer height in three clusters obviously decreased, C1 (−53.58%) and C2 (−48.13%). Obviously, worse diffusion conditions lead to an increase in the PM_{2.5} concentration. The PM_{2.5} concentration in C1 upwind direction is higher than that in SH, while the ozone concentration is lower. The transport of C1 upwind also contributes. In C2, the relative humidity increased by 12.78% which contributed to the hygroscopic growth of PM_{2.5} and a decrease in O₃ production. Less SSR (−20.96%) and higher cloud cover (+24.92%) in C2 were not conducive to the formation of ozone photochemical reactions. The same conditions were found in C3, but it was less obvious than C2, +8.69% for cloud cover and −9.67% for SSR. Thus, transportation and increased relative humidity were also factors that cannot be ignored in C3.

The cause of another seesaw event is not as complicated as that of Type-one events. Figure 6 and Tables 1, 3 show that the moist oceanic air mass with rich O₃ from the northeast sea enters Shanghai and reduces the concentration of PM_{2.5} at the same time in two clusters of Type-two events. Transport is undoubtedly the main influencing factor in both clusters of Type-two events. Adequate precipitation also contributes to the wet removal of fine particles in C1. A doubled BLH (+100.02%) was beneficial to the diffusion of PM_{2.5} in C2. A 6.27% increase in SSR contributed to the photochemical production of O₃ under clear sky conditions.

Except for the production of ozone from photochemical reactions occurring within the troposphere, the presence of ozone in the troposphere is understood to arise from another basic process. Tropospheric-stratospheric exchange can cause the transport of stratospheric air, rich in ozone, into the troposphere (Langford, 1999). Ni et al. suggested that stratospheric ozone intrusion acts as an additional source of the near-surface tropospheric ozone concentration, which deteriorates O₃ pollution in China (Ni et al., 2019).

Therefore, we also made a vertical profile of the ozone mass mixing ratio in autumn (Figure 11). The scavenging process of precipitation can be clearly seen in this figure. Note that when the seesaw events occurred, the near-surface ozone concentration increased, but the ozone concentration in the upper levels decreased. During the precipitation, strong convective weather with obvious downward flow may have affected stratospheric-tropospheric exchange of air masses and ozone concentrations. Therefore, it is also suspected that the near-surface tropospheric ozone concentration is closely related to transport from the upper layer or stratosphere. However, there are currently no further data supporting this hypothesis. Besides autumn, the transport of ozone in the upper and lower layers is not obvious in other seasons.

Data availability statement

The original contributions presented in the study are included in the article/Supplementary Material, further inquiries can be directed to the corresponding author.

Author contributions

XW and YS designed the research. YS performed the analyses and wrote the paper. Both authors contributed to the final version of the paper.

Funding

This research has been supported by the National Natural Science Foundation of China (Grant Nos. 42075058, 41790470 and 41805117) and Shanghai International Science and Technology Partnership Project (No. 21230780200).

Acknowledgments

Daily pollutant concentration observations in Shanghai were obtained from the website of the Ministry of Ecology and

References

- American Meteorological Society American Meteorological Society (2022). Rain".Glossary of meteorology. Available at: <https://glossary.ametsoc.org/wiki/Rain> (Accessed July 16, 2022).
- Andronache, C. (2003). Estimated variability of below-cloud aerosol removal by rainfall for observed aerosol size distributions. *Atmos. Chem. Phys.* 13, 131–143. doi:10.5194/acp-3-131-2003
- Bond, T. C., Doherty, S. J., Fahey, D. W., Forster, P. M., Berntsen, T., DeAngelo, B. J., et al. (2013). Bounding the role of black carbon in the climate system: A scientific assessment. *J. Geophys. Res. Atmos.* 118, 5380–5552. doi:10.1002/jgrd.50171
- Box, J. F. (1987). Guinness, gosset, Fisher, and small samples. *Stat. Sci.* 2, 13437. doi:10.1214/ss/1177013437
- Buchard, V., da Silva, A. M., Randles, C. A., Colarco, P., Ferrare, R., Hair, J., et al. (2016). Evaluation of the surface PM_{2.5} in version 1 of the NASA MERRA aerosol reanalysis over the United States. *Atmos. Environ.* X. 125, 100–111. doi:10.1016/j.atmosenv.2015.11.004
- Camalier, L., Cox, W., and Dolwick, P. (2007). The effects of meteorology on ozone in urban areas and their use in assessing ozone trends. *Atmos. Environ.* X. 41, 7127–7137. doi:10.1016/j.atmosenv.2007.04.061
- Carrillo-Torres, E., Hernández-Paniagua, I., and Mendoza, A. (2017). Use of combined observational- and model-derived photochemical indicators to assess the O₃-NO_x-VOC system sensitivity in urban areas. *Atmosphere* 8, 22. doi:10.3390/atmos8020022
- Chang, L., He, F., Tie, X., Xu, J., and Gao, W. (2021). Meteorology driving the highest ozone level occurred during mid-spring to early summer in Shanghai, China. *Sci. Total Environ.* 785, 147253. doi:10.1016/j.scitotenv.2021.147253
- Charlson, R. J., Schwartz, S. E., Hales, J. M., Cess, R. D., Coakley, J. A., Hansen, J. E., et al. (1992). Climate forcing by anthropogenic aerosols. *Science* 255, 423–430. doi:10.1126/science.255.5043.423
- Environment of the People's Republic of China (<http://106.37.208.233:20035>; MEEPRC, 2022). The 4-hourly ECMWF ERA5 dataset from 2014 to 2020 was downloaded from <https://www.ecmwf.int/en/forecasts/datasets/reanalysis-datasets/era5> (ECMWF, 2022). Backward trajectory analysis was conducted using Hybrid–Single Particle Lagrangian Integrated Trajectory (HYSPLIT), which can be downloaded at <https://www.ready.noaa.gov/HYSPLIT.php>.
- Chate, D. M., Rao, P. S. P., Naik, M. S., Momin, G. A., Safai, P. D., and Ali, K. (2003). Scavenging of aerosols and their chemical species by rain. *Atmos. Environ.* X. 37, 2477–2484. doi:10.1016/S1352-2310(03)00162-6
- Chen, L., Zhu, J., Liao, H., Yang, Y., and Yue, X. (2020). Meteorological influences on PM_{2.5} and O₃ trends and associated health burden since China's clean air actions. *Sci. Total Environ.* 744, 140837. doi:10.1016/j.scitotenv.2020.140837
- Cox, W. M., and Chu, S.-H. (1996). Assessment of interannual ozone variation in urban areas from a climatological perspective. *Atmos. Environ.* X. 30, 2615–2625. doi:10.1016/1352-2310(95)00346-0
- Dang, R., and Liao, H. (2019). Radiative forcing and health impact of aerosols and ozone in China as the consequence of clean air actions over 2012–2017. *Geophys. Res. Lett.* 46, 12511–12519. doi:10.1029/2019GL084605
- Dawson, J. P., Adams, P. J., and Pandis, S. N. (2007). Sensitivity of PM_{2.5} to climate in the eastern US: A modeling case study. *Atmos. Chem. Phys.* 15, 4295–4309. doi:10.5194/acp-7-4295-2007
- Deng, X., Zhou, X., Tie, X., Wu, D., Li, F., Tan, H., et al. (2012). Attenuation of ultraviolet radiation reaching the surface due to atmospheric aerosols in Guangzhou. *Chin. Sci. Bull.* 57, 2759–2766. doi:10.1007/s11434-012-5172-5
- Draxler, R., Stunder, B., Rolph, G., Stein, A., Taylor, A., Zinn, S., et al. (2009). *HYSPLIT User's Guide*, 315. <https://www.ready.noaa.gov/hysplitusersguide/S000.htm>.
- Finlayson-Pitts, B. J., and Pitts, J. (1986). Atmospheric chemistry. Fundamentals and experimental techniques. Available at: <https://www.osti.gov/biblio/6379212> (Accessed June 20, 2022).
- Gao, W., Tie, X., Xu, J., Huang, R., Mao, X., Zhou, G., et al. (2017). Long-term trend of O₃ in a mega City (Shanghai), China: Characteristics, causes, and interactions with precursors. *Sci. Total Environ.* 9, 425–433. doi:10.1016/j.scitotenv.2017.06.099

Conflict of interest

The authors declare that the research was conducted in the absence of any commercial or financial relationships that could be construed as a potential conflict of interest.

Publisher's note

All claims expressed in this article are solely those of the authors and do not necessarily represent those of their affiliated organizations, or those of the publisher, the editors and the reviewers. Any product that may be evaluated in this article, or claim that may be made by its manufacturer, is not guaranteed or endorsed by the publisher.

- Gillani, N. V., and Pleim, J. E. (1996). Sub-grid-scale features of anthropogenic emissions of NOx and VOC in the context of regional eulerian models. *Atmos. Environ. X* 30, 2043–2059. doi:10.1016/1352-2310(95)00201-4
- Gu, Y., Li, K., Xu, J., Liao, H., and Zhou, G. (2020a). Observed dependence of surface ozone on increasing temperature in Shanghai, China. *Atmos. Environ. X* 22, 117108. doi:10.1016/j.atmosenv.2019.117108
- Gu, Y., Yan, F., Xu, J., Qu, Y., Gao, W., He, F., et al. (2020b). A measurement and model study on ozone characteristics in marine air at a remote island station and its interaction with urban ozone air quality in Shanghai, China. *Atmos. Chem. Phys.* 20, 14361–14375. doi:10.5194/acp-20-14361-2020
- Guenther, A., Karl, T., Harley, P., Wiedinmyer, C., Palmer, P. I., and Geron, C. (2006). Estimates of global terrestrial isoprene emissions using MEGAN (model of emissions of gases and aerosols from nature). *Atmos. Chem. Phys.* 30, 3181–3210. doi:10.5194/acp-6-3181-2006
- He, J., Gong, S., Yu, Y., Yu, L., Wu, L., Mao, H., et al. (2017). Air pollution characteristics and their relation to meteorological conditions during 2014–2015 in major Chinese cities. *Environ. Pollut.* 223, 484–496. doi:10.1016/j.envpol.2017.01.050
- He, L., Lin, A., Chen, X., Zhou, H., Zhou, Z., and He, P. (2019). Assessment of MERRA-2 surface PM_{2.5} over the Yangtze River basin: Ground-based verification, spatiotemporal distribution and meteorological dependence. *Remote Sens. (Basel)* 11, 460. doi:10.3390/rs11040460
- He, S., and Carmichael, G. R. (1999). Sensitivity of photolysis rates and ozone production in the troposphere to aerosol properties. *J. Geophys. Res.* 104, 26307–26324. doi:10.1029/1999JD900789
- Hersbach, H., Bell, B., Berrisford, P., Hirahara, S., Horányi, A., Muñoz-Sabater, J., et al. (2020). The ERA5 global reanalysis. *Q. J. R. Meteorol. Soc.* 146, 1999–2049. doi:10.1002/qj.3803
- Hu, J., Wu, L., Zheng, B., Zhang, Q., He, K., Chang, Q., et al. (2015). Source contributions and regional transport of primary particulate matter in China. *Environ. Pollut.* 207, 31–42. doi:10.1016/j.envpol.2015.08.037
- Jacob, D. J., and Winner, D. A. (2009). Effect of climate change on air quality. *Atmos. Environ.* 43, 51–63. doi:10.1016/j.atmosenv.2008.09.051
- Jacobson, M. Z. (1998). Studying the effects of aerosols on vertical photolysis rate coefficient and temperature profiles over an urban airshed. *J. Geophys. Res.* 103, 10593–10604. doi:10.1029/98JD00287
- Jia, M., Zhao, T., Cheng, X., Gong, S., Zhang, X., Tang, L., et al. (2017). Inverse relations of PM_{2.5} and O₃ in air compound pollution between cold and hot seasons over an urban area of east China. *Atmosphere* 8, 59. doi:10.3390/atmos8030059
- Johnson, C. E., Collins, W. J., Stevenson, D. S., and Derwent, R. G. (1999). Relative roles of climate and emissions changes on future tropospheric oxidant concentrations. *J. Geophys. Res.* 104, 18631–18645. doi:10.1029/1999JD900204
- Kleinman, L. I., Daum, P. H., Lee, Y.-N., Nunnermacker, L. J., Springston, S. R., Weinstein-Lloyd, J., et al. (2003). Photochemical age determinations in the phoenix metropolitan area: Photochemical age determinations in phoenix. *J. Geophys. Res.* 108, 2621. doi:10.1029/2002JD002621
- Kley, D. (1997). Tropospheric chemistry and transport. *Science* 276, 1043–1044. doi:10.1126/science.276.5315.1043
- Langford, A. O. (1999). Stratosphere-troposphere exchange at the subtropical jet: Contribution to the tropospheric ozone budget at midlatitudes. *Geophys. Res. Lett.* 26, 2449–2452. doi:10.1029/1999GL900556
- Li, G., Bei, N., Tie, X., and Molina, L. T. (2011). Aerosol effects on the photochemistry in Mexico City during MCMA-2006/MILAGRO campaign. *Atmos. Chem. Phys.* 11, 5169–5182. doi:10.5194/acp-11-5169-2011
- Li, K., Jacob, D. J., Liao, H., Qiu, Y., Shen, L., Zhai, S., et al. (2021). Ozone pollution in the North China Plain spreading into the late-winter haze season. *Proc. Natl. Acad. Sci. U. S. A.* 118, e2015797118. doi:10.1073/pnas.2015797118
- Li, K., Jacob, D. J., Liao, H., Shen, L., Zhang, Q., and Bates, K. H. (2019). Anthropogenic drivers of 2013–2017 trends in summer surface ozone in China. *Proc. Natl. Acad. Sci. U. S. A.* 116, 422–427. doi:10.1073/pnas.1812168116
- Li, K., Jacob, D. J., Shen, L., Lu, X., De Smedt, I., and Liao, H. (2020). Increases in surface ozone pollution in China from 2013 to 2019: Anthropogenic and meteorological influences. *Atmos. Chem. Phys.* 20, 11423–11433. doi:10.5194/acp-20-11423-2020
- Liu, H., Liu, S., Xue, B., Lv, Z., Meng, Z., Yang, X., et al. (2018). Ground-level ozone pollution and its health impacts in China. *Atmos. Environ. X* 173, 223–230. doi:10.1016/j.atmosenv.2017.11.014
- Liu, Y., and Wang, T. (2020a). Worsening urban ozone pollution in China from 2013 to 2017 – Part 1: The complex and varying roles of meteorology. *Atmos. Chem. Phys.* 20, 6305–6321. doi:10.5194/acp-20-6305-2020
- Liu, Y., and Wang, T. (2020b). Worsening urban ozone pollution in China from 2013 to 2017 – Part 2: The effects of emission changes and implications for multi-pollutant control. *Atmos. Chem. Phys.* 20, 6323–6337. doi:10.5194/acp-20-6323-2020
- Lu, X., Zhang, L., Chen, Y., Zhou, M., Zheng, B., Li, K., et al. (2019a). Exploring 2016–2017 surface ozone pollution over China: Source contributions and meteorological influences. *Atmos. Chem. Phys.* 19, 8339–8361. doi:10.5194/acp-19-8339-2019
- Lu, X., Zhang, L., and Shen, L. (2019b). Meteorology and climate influences on tropospheric ozone: A review of natural sources, chemistry, and transport patterns. *Curr. Pollut. Rep.* 5, 238–260. doi:10.1007/s40726-019-00118-3
- Ministry of Ecology and Environment (2013). Ministry of Ecology and Environment: Technical Specifications for Installation and Acceptance of Ambient Air Quality Continuous Automated Monitoring System for SO₂, NO₂, O₃ and CO. Available at: <http://www.mee.gov.cn/ywqz/fgbz/bz/bzwb/jcffbz/201308/W020130802493970989627.pdf> (Accessed July 16, 2022).
- Ministry of Ecology and Environment (2022). Technical Specification for Environmental Air Quality Assessment (Trial). Available at: http://www.mee.gov.cn/ywqz/fgbz/bz/bzwb/jcffbz/201309/t20130925_260809.shtml (Accessed July 16, 2022).
- Ministry of Ecology and Environment (2012). Ministry of Ecology and Environment: Ambient Air Quality Standards. Available at: https://english.mee.gov.cn/Resources/standards/Air_Environment/quality_standard1/201605/t20160511_337502.shtml (Accessed July 16, 2022).
- Mu, M., and Zhang, R. (2014). Addressing the issue of fog and haze: A promising perspective from meteorological science and technology. *Sci. China Earth Sci.* 57, 1–2. doi:10.1007/s11430-013-4791-2
- Ni, Z.-Z., Luo, K., Gao, X., Gao, Y., Fan, J.-R., Fu, J. S., et al. (2019). Exploring the stratospheric source of ozone pollution over China during the 2016 Group of Twenty summit. *Atmos. Pollut. Res.* 10, 1267–1275. doi:10.1016/j.apr.2019.02.010
- Shan, W., Yin, Y., Zhang, J., and Ding, Y. (2008). Observational study of surface ozone at an urban site in East China. *Atmos. Res.* 89, 252–261. doi:10.1016/j.atmosres.2008.02.014
- Shao, P., Xin, J., Zhang, X., Gong, C., Ma, Y., Wang, Y., et al. (2022). Aerosol optical properties and their impacts on the co-occurrence of surface ozone and particulate matter in Kunming City, on the Yunnan–Guizhou Plateau of China. *Atmos. Res.* 266, 105963. doi:10.1016/j.atmosres.2021.105963
- Sillman, S., Logan, J. A., and Wofsy, S. C. (1990). The sensitivity of ozone to nitrogen oxides and hydrocarbons in regional ozone episodes. *J. Geophys. Res.* 95, 1837. doi:10.1029/JD095iD02p01837
- Sillman, S. (1999). The relation between ozone, NOx and hydrocarbons in urban and polluted rural environments. *Atmos. Environ.* 25.
- Silver, B., Reddington, C. L., Arnold, S. R., and Spracklen, D. V. (2018). Substantial changes in air pollution across China during 2015–2017. *Environ. Res. Lett.* 13, 114012. doi:10.1088/1748-9326/aae718
- Simon, H., Reff, A., Wells, B., Xing, J., and Frank, N. (2015). Ozone trends across the United States over a period of decreasing NOx and VOC emissions. *Environ. Sci. Technol.* 49, 186–195. doi:10.1021/es504514z
- Sirois, A., and Bottenheim, J. W. (1995). Use of backward trajectories to interpret the 5-year record of PAN and O₃ ambient air concentrations at Kejimikujik National Park, Nova Scotia. *J. Geophys. Res.* 100, 2867. doi:10.1029/94JD02951
- State Council of the People's Republic of China (2018). State Council of the People's Republic of China: Notice of the state Council on printing and distributing the three-year action plan for winning the blue sky defense war. Available at: http://www.gov.cn/zhengce/content/2018-07/03/content_5303158.htm (Accessed July 16, 2022).
- Su, T., Li, Z., and Kahn, R. (2018). Relationships between the planetary boundary layer height and surface pollutants derived from lidar observations over China: Regional pattern and influencing factors. *Atmos. Chem. Phys.* 18, 15921–15935. doi:10.5194/acp-18-15921-2018
- Tie, X., Geng, F., Guenther, A., Cao, J., Greenberg, J., Zhang, R., et al. (2013). Megacity impacts on regional ozone formation: Observations and WRF-chem modeling for the MIRAGE-shanghai field campaign. *Atmos. Chem. Phys.* 13, 5655–5669. doi:10.5194/acp-13-5655-2013
- Tie, X., Madronich, S., Li, G., Ying, Z., Weinheimer, A., Apel, E., et al. (2009). Simulation of Mexico City plumes during the MIRAGE-Mex field campaign using the WRF-Chem model. *Atmos. Chem. Phys.* 18, 4621–4638. doi:10.5194/acp-9-4621-2009
- Wang, X., and Wang, K. (2016). Homogenized variability of radiosonde-derived atmospheric boundary layer height over the global land surface from 1973 to 2014. *J. Climate* 29 (19), 6893–6908. doi:10.1175/JCLI-D-15-0766.1
- Wang, X., and Wang, K. (2014). Estimation of atmospheric mixing layer height from radiosonde data. *Atmos. Measurement Tech.* 7 (2). doi:10.5194/amt-7-1701-2014
- Wang, W., Li, X., Shao, M., Hu, M., Zeng, L., Wu, Y., et al. (2019a). The impact of aerosols on photolysis frequencies and ozone production in Beijing during the 4-year period 2012–2015. *Atmos. Chem. Phys.* 19, 9413–9429. doi:10.5194/acp-19-9413-2019

- Wang, X., Dickinson, R. E., Su, L., Zhou, C., and Wang, K. (2018). PM_{2.5} pollution in China and how it has been exacerbated by terrain and meteorological conditions. *Bull. Am. Meteorol. Soc.* 99, 105–119. doi:10.1175/BAMS-D-16-0301.1
- Wang, X., Wang, K., and Su, L. (2016). Contribution of atmospheric diffusion conditions to the recent improvement in air quality in China. *Sci. Rep.* 6, 36404. doi:10.1038/srep36404
- Wang, X., Zhang, L., and Moran, M. D. (2010). Uncertainty assessment of current size-resolved parameterizations for below-cloud particle scavenging by rain. *Atmos. Chem. Phys.* 10, 5685–5705. doi:10.5194/acp-10-5685-2010
- Wang, X., and Zhang, R. (2020). How did air pollution change during the COVID-19 outbreak in China? *Bull. Am. Meteorol. Soc.* 101, E1645–E1652. doi:10.1175/BAMS-D-20-0102.1
- Wang, X., Zhang, R., Tan, Y., and Yu, W. (2021). Dominant synoptic patterns associated with the decay process of PM_{2.5} pollution episodes around Beijing. *Atmos. Chem. Phys.* 21, 2491–2508. doi:10.5194/acp-21-2491-2021
- Wang, X., Zhang, R., and Yu, W. (2019b). The effects of PM_{2.5} concentrations and relative humidity on atmospheric visibility in Beijing. *J. Geophys. Res. Atmos.* 124, 2235–2259. doi:10.1029/2018JD029269
- Won, W.-S., Oh, R., Lee, W., Ku, S., Su, P.-C., and Yoon, Y.-J. (2021). Hygroscopic properties of particulate matter and effects of their interactions with weather on visibility. *Sci. Rep.* 11, 16401. doi:10.1038/s41598-021-95834-6
- Wu, X., Xin, J., Zhang, W., Gao, W., Ma, Y., Ma, Y., et al. (2022). Variation characteristics of air combined pollution in Beijing City. *Atmos. Res.* 274, 106197. doi:10.1016/j.atmosres.2022.106197
- Xiao, Q., Ma, Z., Li, S., and Liu, Y. (2015). The impact of winter heating on air pollution in China. *PLOS ONE* 10, e0117311. doi:10.1371/journal.pone.0117311
- Xu, D., Yap, D., and Taylor, P. A. (1996). Meteorologically adjusted ground level ozone trends in Ontario. *Atmos. Environ.* 30, 1117–1124. doi:10.1016/1352-2310(95)00331-2
- Yin, Z., Li, Y., and Cao, B. (2020). Seasonal prediction of surface O₃-related meteorological conditions in summer in North China. *Atmos. Res.* 246, 105110. doi:10.1016/j.atmosres.2020.105110
- Yin, Z., Wang, H., and Chen, H. (2017). Understanding severe winter haze events in the north China plain in 2014: Roles of climate anomalies. *Atmos. Chem. Phys.* 17, 1641–1651. doi:10.5194/acp-17-1641-2017
- Yue, X., Unger, N., Harper, K., Xia, X., Liao, H., Zhu, T., et al. (2017). Ozone and haze pollution weakens net primary productivity in China. *Atmos. Chem. Phys.* 17, 6073–6089. doi:10.5194/acp-17-6073-2017
- Zhai, S., Jacob, D. J., Wang, X., Shen, L., Li, K., Zhang, Y., et al. (2019). Fine particulate matter (PM_{2.5}) trends in China, 2013–2018: Separating contributions from anthropogenic emissions and meteorology. *Atmos. Chem. Phys.* 19, 11031–11041. doi:10.5194/acp-19-11031-2019
- Zhang, R., Li, Q., and Zhang, R. (2014). Meteorological conditions for the persistent severe fog and haze event over eastern China in January 2013. *Sci. China Earth Sci.* 57, 26–35. doi:10.1007/s11430-013-4774-3
- Zhang, R. (2017). Warming boosts air pollution. *Nat. Clim. Chang.* 7, 238–239. doi:10.1038/nclimate3257
- Zhang, Y.-L., and Cao, F. (2015). Fine particulate matter (PM_{2.5}) in China at a city level. *Sci. Rep.* 5, 14884. doi:10.1038/srep14884
- Zhong, Q., Tao, S., Ma, J., Liu, J., Shen, H., Shen, G., et al. (2021). PM_{2.5} reductions in Chinese cities from 2013 to 2019 remain significant despite the inflating effects of meteorological conditions. *One Earth* 4, 448–458. doi:10.1016/j.oneear.2021.02.003
- Zhu, B., Kang, H., Zhu, T., Su, J., Hou, X., and Gao, J. (2015). Impact of Shanghai urban land surface forcing on downstream city ozone chemistry: Urban land-surface forcing on ozone. *J. Geophys. Res. Atmos.* 120, 4340–4351. doi:10.1002/2014JD022859
- Zhu, J., Chen, L., Liao, H., and Dang, R. (2019). Correlations between PM_{2.5} and ozone over China and associated underlying reasons. *Atmosphere* 10, 352. doi:10.3390/atmos10070352